Chemistry–A European Journal
Research Article
doi.org/10.1002/chem.202303107
Chemistry Europe
European Chemical Societies Publishing
www.chemeurj.org

Hot Paper

Special Collection

Self-Assembly of Discrete Oligomers of Naphthalenediimides in Bulk and on Surfaces

Christiaan H. W. A. Corbet,[a] Bart W. L. van den Bersselaar,[a] Bas F. M. de Waal,[a] Robby Reynaerts,[b] Kunal S. Mali,[b] Steven De Feyter,[b] Alain M. Jonas,[c] E. W. Meijer,*[a, d] and Ghislaine Vantomme*[a]

Here, we report on the synthesis of discrete oligomers of alkyl-bridged naphthalenediimides (NDIs) and study their molecular nanostructures both in bulk, in solution, and at the liquid-solid interface. Via an iterative synthesis method, multiple NDI cores were bridged with short and saturated alkyl-diamines (C_3 and C_{12}) or long and unsaturated alkyl-diamines (u_2C_{33} to u_8C_{100}) at their imide termini. The strong intermolecular interaction between the NDI cores was observed by probing their photophysical properties in solution. In bulk, the discrete NDI oligomers preferentially ordered in lamellar morphologies, irrespective of whether a saturated or unsaturated spacer was employed. Moreover, both the molecular architecture as well as the crystallization conditions play a significant role in the nanoscale ordering. The long unsaturated alkyl chains lead preferably to folded-chain conformations while their saturated analogues form stretched arrangements. At the solution-solid interface, well-defined lamellar regions were observed. These results show that precision in chemical structure alone is not sufficient to reach well-defined structures of discrete oligomers, but that it must be combined with precision in processing conditions.

Introduction

When organic and polymer chemistry join forces, oligomeric materials that are perfectly defined at the molecular level can be synthesized.[1] This class of materials has shown unprecedented properties linked to their well-defined nanostructures, making them exciting targets for nanotechnology.[2–5] In fact, by the controlled assembly of discrete structures, molecular events can be amplified from the nano- to the macroscopic scale and lead to distinct function.[6–8] However, the preparation of precise oligomer materials requires a great synthetic effort, either by iterative, multi-step syntheses or by the separation of disperse oligomeric mixtures. Therefore, the examples of precision oligomer materials with a molar mass dispersity $Đ < 1.0001$ are rather scarce. This raises the question of the trade-off between synthetic efforts and novel properties in these molecularly perfect materials, not only in bulk but also at the liquid-solid interface.

A well-studied moiety in structured materials and suitable candidate for precise oligomer materials is naphthalenediimide (NDI). NDIs are electron-poor, π-conjugated chromophores and exhibit strong intermolecular interactions.[9,10] They are versatile due to their high synthetic accessibility and tunability and can thereby be optimized for a desired purpose. These units can be functionalized either at the imide nitrogen or at the naphthalene core, which results in variable photophysical and electronic properties.[9] For these reasons, NDIs have been studied extensively, in various fields of research, such as field-effect transistors, thin film semiconductors and in charge-transfer complex systems,[11–16] but also in DNA systems and in hydrogels.[17–19] In supramolecular systems, small molecules with one NDI core[20,21] or polymers with multiple NDI cores have been reported.[22,23] In a few examples, discrete multimeric NDI molecules have been studied in foldamers[24,25] and for (opto)electronics[26,27] and sensing,[28] showing their potential as precise oligomer materials.

Recently, two types of discrete NDI-based block co-oligomers were studied in bulk and at the liquid-solid interface, with oligo-dimethylsiloxane[29,30] and alkane[31,32] spacers. Both the molecular architecture and the length of the spacers were

[a] C. H. W. A. Corbet, B. W. L. van den Bersselaar, B. F. M. de Waal, Prof. Dr. E. W. Meijer, Dr. G. Vantomme
Institute for Complex Molecular Systems and Laboratory of Macromolecular and Organic Chemistry, Department of Chemical Engineering and Chemistry
Eindhoven University of Technology
P.O. Box 513, 5600 MB Eindhoven (The Netherlands)
E-mail: e.w.meijer@tue.nl
g.vantomme@tue.nl
[b] R. Reynaerts, Dr. K. S. Mali, Prof. Dr. S. De Feyter
Division of Molecular Imaging and Photonics, Department of Chemistry
KU Leuven
Celestijnenlaan 200 F, B-3001 Leuven (Belgium)
[c] Prof. Dr. A. M. Jonas
Institute of Condensed Matter and Nanosciences, Bio- and Soft Matter
Université catholique de Louvain-UCLouvain
Ottignies-Louvain-la-Neuve, Louvain-la-Neuve B-1348 (Belgium)
[d] Prof. Dr. E. W. Meijer
School of Chemistry and RNA Institute,
University of New South Wales
Sydney (Australia)

Supporting information for this article is available on the WWW under https://doi.org/10.1002/chem.202303107

Part of a Special Collection celebrating the 120th anniversary of the Royal Netherlands Chemical Society

varied and showed a large impact on the obtained morphologies. The crystallinity of the NDIs and the phase separation between the two blocks were shown to drive the assembly of the well-defined nanostructures in bulk. Moreover, these structures were assembled at the 1-phenyloctane/highly oriented pyrolytic graphite (HOPG) interface and it was found that monolayers of the unsaturated compounds mostly resulted in larger well-ordered domains compared to the saturated counterparts.[33,34]

Encouraged by these interesting results on the assembly of NDIs, we herein explore the synthesis and assembly properties of discrete NDI dimers, trimers, tetramers and pentamers spaced by various saturated and unsaturated alkyl chains (Figure 1). We investigate their synthetic accessibility, solubility, processability and long-range assembly by varying the linker length, degree of polymerization and sequence. The molecular structures were characterized by NMR, MALDI-ToF-MS and FT-IR spectroscopy. For the structural characterization in bulk and in solution, differential scanning calorimetry (DSC), polarized optical microscopy (POM), small-angle X-ray scattering (SAXS) and UV-vis absorption and fluorescence spectroscopy were used. Finally, the formation of assembled 2D monolayers was investigated on liquid/HOPG interface by means of scanning tunneling microscopy (STM).

Results and Discussion

Synthesis and characterization

Three sets of NDI oligomers were synthesized via an iterative synthetic approach (Schemes 1 and 2). The first set consists of two NDI trimers, **C_3-NDI$_3$** and **C_{12}-NDI$_3$**, where the spacer between the NDI cores is a propyl or a dodecyl chain respectively. For the second and third set, NDI oligomers with discrete unsaturated alkane spacers were synthesized because this spacer was expected to substantially improve the processability and solubility in organic solvents. In the second set, an alternating block co-oligomer was designed, where the number of NDI units was varied from two to five units (**u$_2$C$_{34}$-NDI$_2$**, **u$_2$C$_{33}$-NDI$_3$** and **u$_2$C$_{33}$-NDI$_5$**). Here, the dimer NDI has a 34-carbon chain length compared to 33-carbon chain length of the trimer and pentamer NDI oligomers, as this was synthetically more accessible. Lastly, the third set consists of varying unsaturated alkane spacers (from 34- to 100-carbon chains) flanked by two

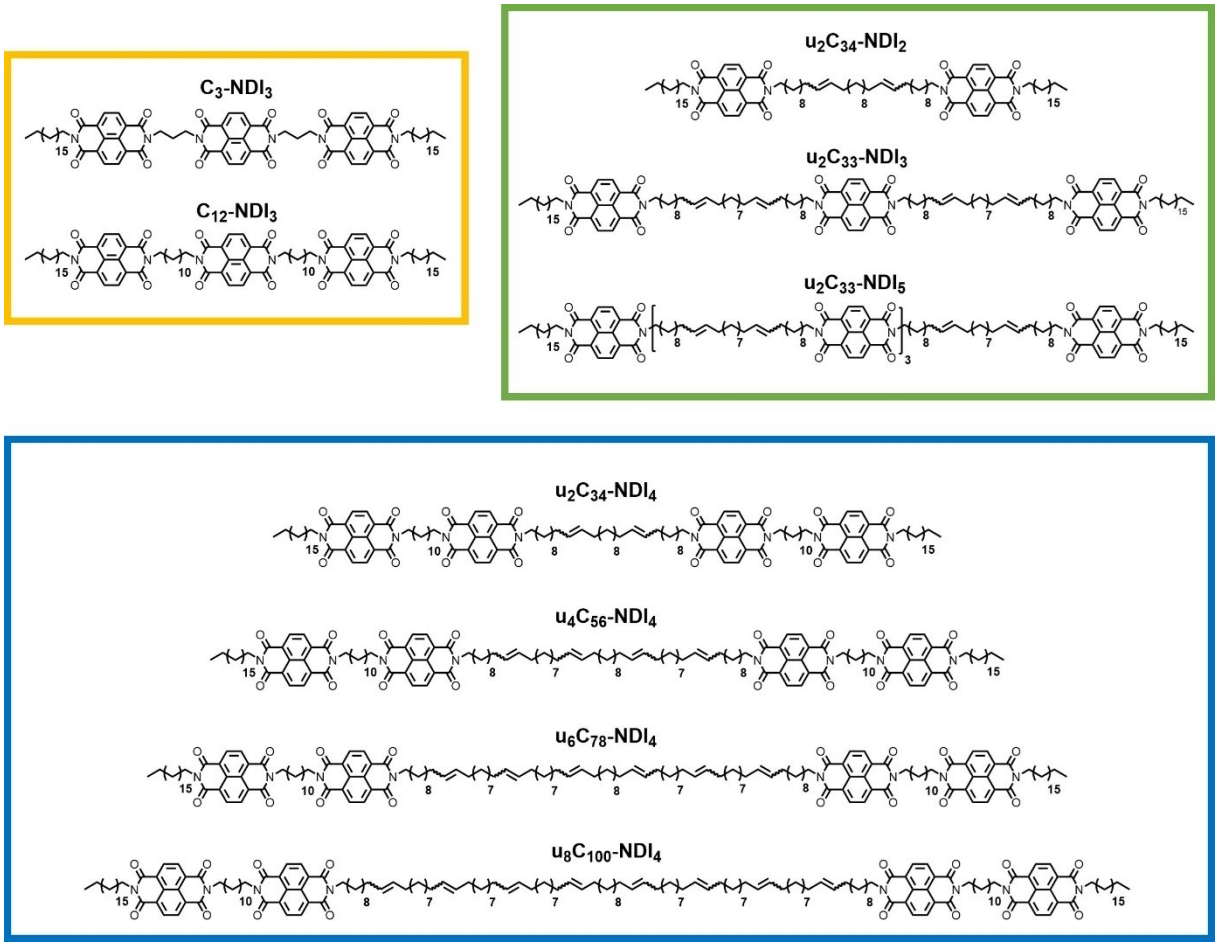

Figure 1. Molecular structures of NDI oligomers with saturated linkers (set 1, orange), alternating NDIs with unsaturated linkers (set 2, green) and peripheral NDIs connected with unsaturated linkers of various sizes (set 3, blue).

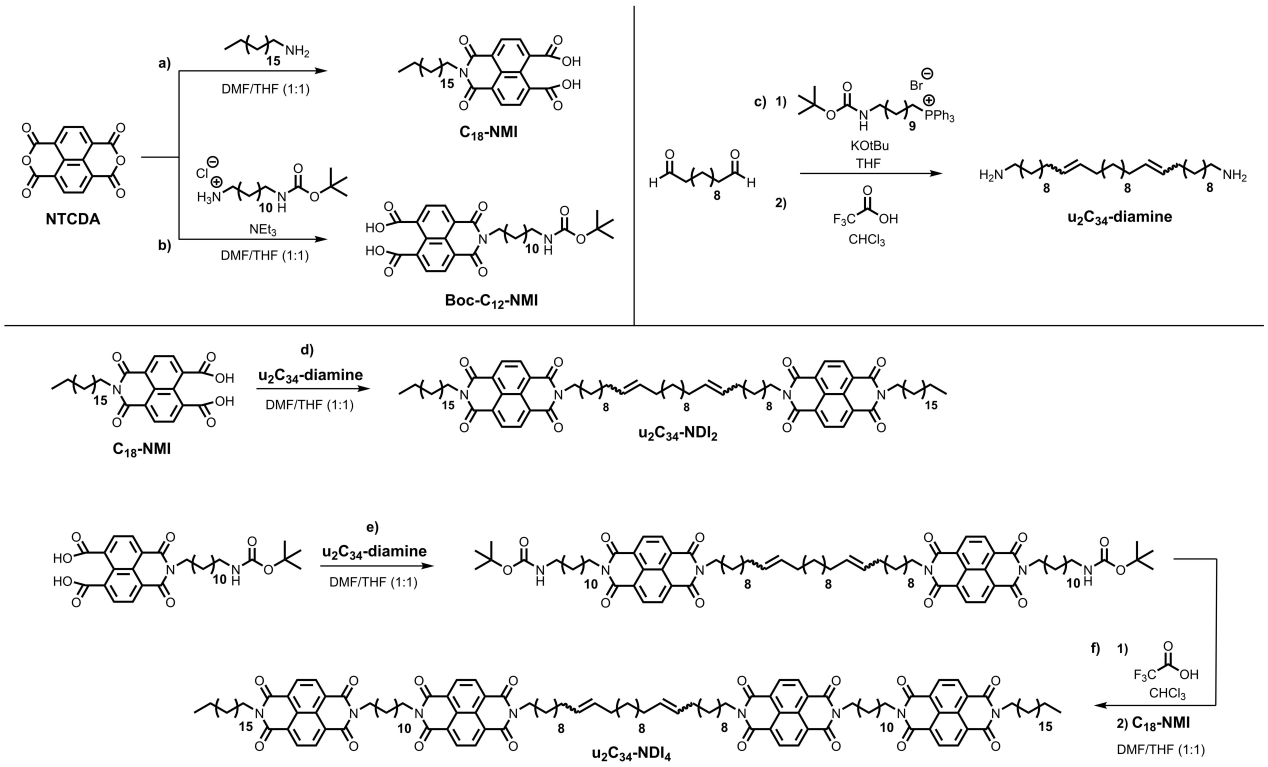

Scheme 1. Synthetic route towards three key intermediates and the subsequent synthesis of NDI oligomers $\mathbf{u_2C_{34}}$**-NDI**$_2$ and $\mathbf{u_2C_{34}}$**-NDI**$_4$ starting from these key intermediates. Reagents and conditions: (a and b) 2.5 eq NTCDA, 1 eq amine, NEt_3 (b only) 50/50 DMF/THF, 75–140 °C, 10 min (88% and 78%); (c) 1) 1,12-dodecandial, phosphonium-salt, KOtBu, THF, 0–20 °C, 24 h, 2) TFA, $CHCl_3$, 20 °C, 24 h (62%); (d) $\mathbf{C_{18}}$**-NMI**, $\mathbf{u_2C_{34}}$**-diamine**, 50/50 DMF/THF, 75–140 °C, 50 min (76%); (e) **Boc-**$\mathbf{C_{12}}$**-NMI**, $\mathbf{u_2C_{34}}$**-diamine**, 50/50 DMF/THF, 75–140 °C, 25 min (77%); (f) 1) **Boc-**$\mathbf{u_2C_{34}}$**-NDI**$_2$, TFA, $CHCl_3$, 20 °C, 24 h, 2) $\mathbf{C_{18}}$**-NMI**, 50/50 DMF/THF, 75–140 °C, 25 min (82%).

NDI cores linked by a dodecyl chain ($\mathbf{u_2C_{34}}$**-NDI**$_4$, $\mathbf{u_4C_{56}}$**-NDI**$_4$, $\mathbf{u_6C_{78}}$**-NDI**$_4$ and $\mathbf{u_8C_{100}}$**-NDI**$_4$). In all oligomers, $\mathbf{u}_x$ denotes the number of unsaturated bonds present in the structure, $\mathbf{C}_y$ the longest carbon chain length between the NDI cores and $\mathbf{NDI}_n$ the number of NDI cores present in the molecule.

In Scheme 1, the synthetic route towards a few key intermediates and their respective NDI oligomers is shown. In this study, the designed NDIs were obtained using a microwave-assisted protocol,[35] where commercially available 1,4,5,8-naphthalenetetracarboxylic dianhydride (NTCDA) was reacted with either an alkyl-monoamine or alkyl-diamine. Key intermediates required for this iterative synthesis were the unsaturated alkyl-diamine linkers and three naphthalene monoimides (NMIs). The NMIs were isolated by using an excess NTCDA in a microwave reaction with either octadecylamine, *N*-Boc-1,12-dodecyldiamine or double unsaturated *N*-Boc-1,33-tritriacontyldiamine (a tritriacontamer consists of 33 repeating units). The remaining anhydrides were hydrolyzed by stirring the reaction mixture in an NaOH solution. The insoluble NMI was isolated by filtration and the carboxylate groups were subsequently acidified with HCl to promote the condensation reaction in the following step. The ability to isolate the NMIs allows for the synthesis of asymmetric NDIs and thus as a building block for the discrete oligomer synthesis. The synthesis of the discrete unsaturated alkyldiamines was based on a modified Wittig olefination protocol (*vide supra*, Scheme 1).[36] As observed previously with similar unsaturated alkyldiamines, the double bonds were formed preferably in the *cis*-configuration.[33,34] The Wittig olefination resulted in a mixture of inseparable *cis*- and *trans*-isomers of which the ratio was quantified by ^{13}C NMR.

As multiple unique discrete NDI oligomers were targeted, multiple synthesis routes were explored. The fastest and smoothest route to obtain discrete NDI oligomers was to build up the molecule from the center (Scheme 2), starting with either the NTCDA unit for odd-numbered NDI oligomers, or an alkyldiamine for even-numbered NDI oligomers. This way, two NDI cores could be added to the starting material in each iterative cycle. All discrete NDI oligomers were purified using either column chromatography or precipitation, depending on the solubility of the oligomer. After drying, all NDI oligomers were obtained as brittle solids.

All NDI oligomers were studied in dilute solutions in various solvents to determine their UV-vis absorbance and fluorescence properties (Figures S1–S3). The absorption spectra show the typical pattern associated with NDIs in a monomeric state, indicating a low propensity for NDI aggregation. Nevertheless, the emission spectra in bad solvents show strong, and broad excimer emission bands originating from pre-associated aggregates in the ground state.

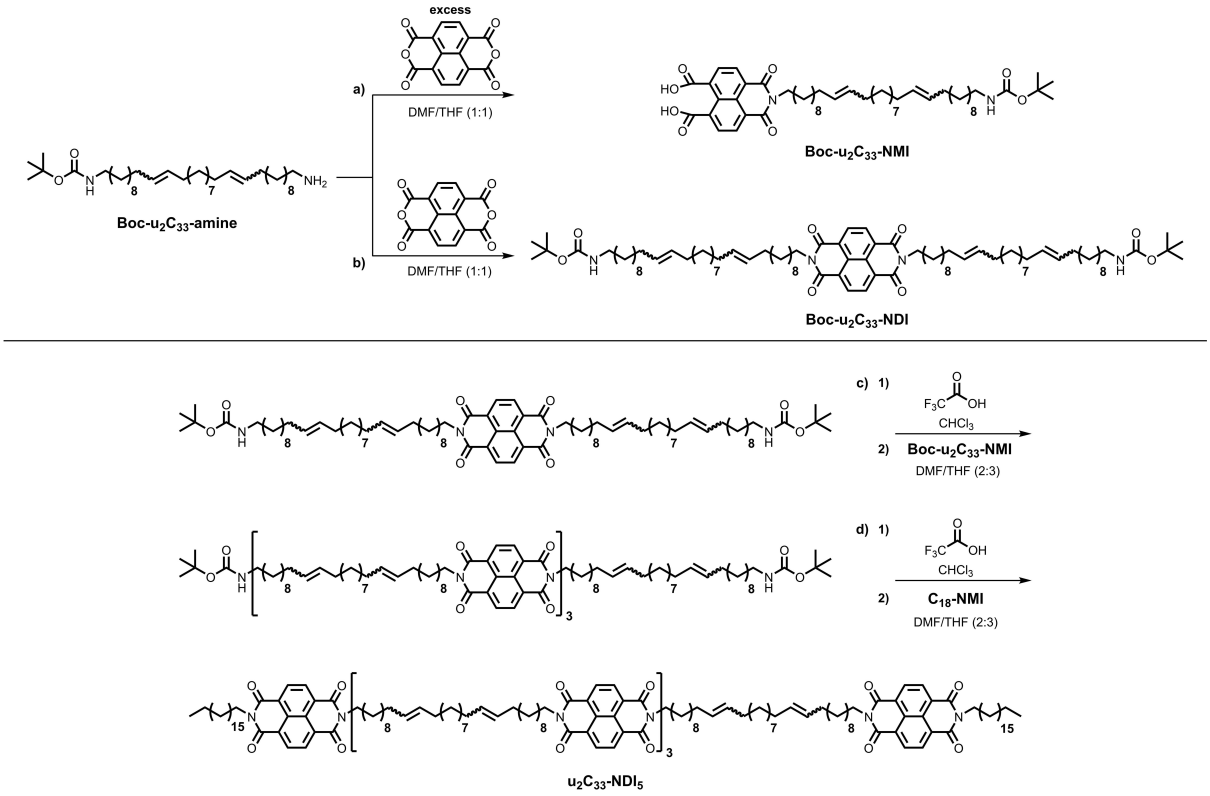

Scheme 2. The iterative synthetic route towards **u_2C_{33}-NDI$_5$** and the synthesis of its precursors. Reagents and conditions: (a) 2.5 eq NTCDA, 1 eq amine, 50/50 DMF/THF, 75–140 °C, 20 min (76%); (b) 1 eq NTCDA, 2.1 eq amine, 50/50 DMF/THF, 75–140 °C, 25 min (90%); (c) 1) **Boc-u_2C_{33}-NDI**, TFA, $CHCl_3$, 20 °C, 20 h, 2) **Boc-u_2C_{33}-NMI**, 40/60 DMF/THF, 75–140 °C, 25 min (60%); (d) 1) **Boc-u_2C_{33}-NDI$_3$**, TFA, $CHCl_3$, 20 °C, 20 h, 2) **C_{18}-NMI**, 40/60 DMF/THF, 75–140 °C, 25 min (19%).

Thermal properties of NDI oligomers in bulk

The thermal properties of the NDI oligomers were investigated using DSC (Figure 2, Table 1). Moreover, variable temperature POM was used to visualize the thermal transitions. The thermal transitions of the pristine unsaturated diamines were recorded as reference data (Figure S4). Upon heating the NDI oligomers, we observed similitudes between the thermal transitions in each set. All but **C_3-NDI$_3$** showed a melting transition T_m and a crystallization transition T_c between 100 °C and 275 °C. **C_3-NDI$_3$** was subjected to temperatures as high as 400 °C under the POM but no isotropic melt was observed. For all NDI oligomers, high enthalpy values corresponding to T_m were measured, suggesting that these molecules are (partly) crystalline solids.

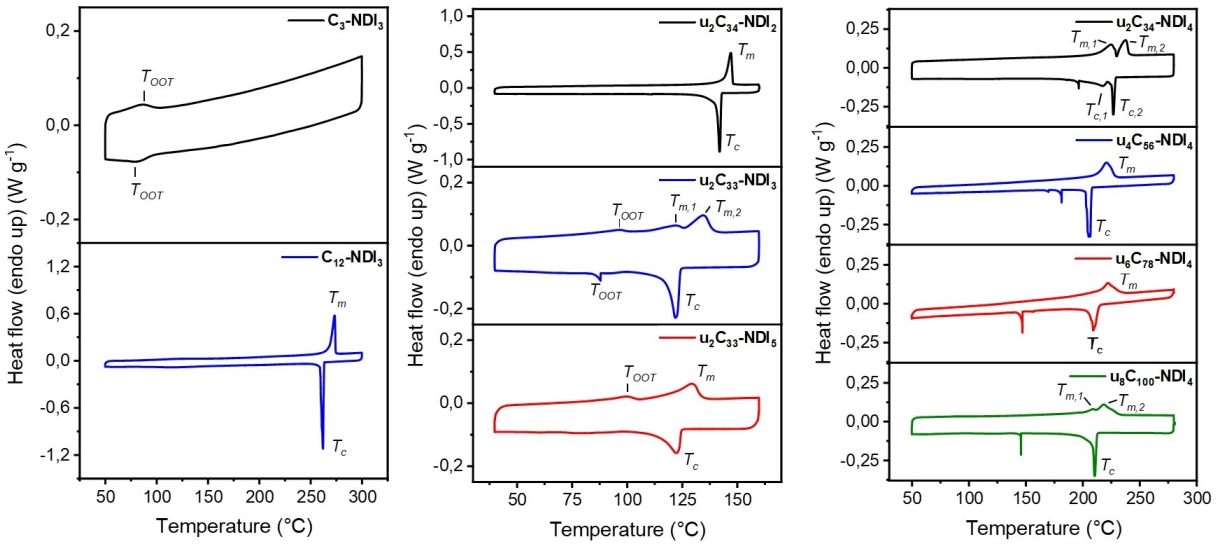

Figure 2. Thermal transitions recorded of all NDI oligomers in the second heating and cooling cycle at a heating/cooling rate of 2 K min^{-1}.

Table 1. Summarized data of the thermal transitions in the NDI oligomers and their enthalpy values.

Entry	Compound	T_{OOT} [°C]	ΔH_{OOT} [kJ/mol]	T_m [°C]	ΔH_{fus} [kJ/mol]	T_c [°C]
1	C_3-NDI_3	85.8	9.3	n.o.	–	n.o.
2	C_{12}-NDI_3	131.4	2.8	273.4	98.6	256.9
3	u_2C_{34}-NDI_2	n.o.	–	147.1	52.4	142.0
4	u_2C_{33}-NDI_3	96.4	2.5	134.7	22.0	121.8
5	u_2C_{33}-NDI_5	99.6	7.8	129.3	55.9	122.4
6	u_2C_{34}-NDI_4	n.o.	–	237.5	48.9	226.8
7	u_4C_{56}-NDI_4	n.o.	–	220.7	73.8	206.4
8	u_6C_{78}-NDI_4	n.o.	–	222.4	77.0	209.1
9	u_8C_{100}-NDI_4	n.o.	–	218.6	41.5	210.3

Many NDI oligomers show smaller endothermic and exothermic transitions below T_m and T_c, which did not result in a change in birefringence in the POM images. Moreover, the material remained un-shearable, hence we ascribed these endo- and exotherms to order-order transitions (OOT) attributed to changes in folded-chain conformation.[37]

Surprisingly, only two NDI oligomers, **C_{12}-NDI_3** and **u_2C_{34}-NDI_2**, show both a sharp T_m and T_C. The combination of their high enthalpy of fusion and sharp transitions suggests that these two oligomers are highly ordered at the molecular level and have therefore been studied for surface self-assembly (*vide infra*). The remaining NDI oligomers, except **C_3-NDI_3**, all display a broad T_m, with **u_2C_{33}-NDI_3**, **u_2C_{34}-NDI_4** and **u_8C_{100}-NDI_4** showing multiple endothermic transitions. The broad melting and crystallization peaks are unexpected, as we anticipated that these NDI oligomers would melt uniformly due to their discrete length. Nonetheless, all the NDI oligomers that show broad T_m and T_c contain *cis-trans* isomers of the unsaturated bond. Consequently, multiple stable folded-chain conformations can exist in bulk, which are prone to have unique melting or crystallization temperatures. This point is further analyzed by SAXS (*vide infra*).

Noticeably, a significant disparity is observed in the melting temperatures of the oligomers between the three sets, attributed to the different architectures of the oligomers and position of the unsaturated bonds in the structure. The fully saturated **C_{12}-NDI_3** has a high T_m of 273 °C, which is comparable to other linear *n*-alkyl single-core NDI molecules and NDI dimers.[31] The unsaturated alkyl-NDI oligomers from the second set have considerably lower T_m varying from 129–147 °C whilst the oligomers of the third set exhibit intermediate values for T_m, varying from 218–238 °C. The decrease in T_m when moving from set 1 to set 2 is explained by the introduction of unsaturated bonds. It is well-known in the literature that molecules comprising unsaturated alkyl chains exhibit a lower T_m than their saturated counterparts.[38,39] To explain the difference between set 2 and set 3, we investigate the alkyl chains that are linked to the NDI cores more closely. In set 2, the NDI cores are directly attached to at least one unsaturated chain, which means that folding can occur between each NDI core. In set 3, the periphery is more crystalline due to the saturated dodecyl spacer between the NDI cores, which results in a higher T_m.

Molecular ordering of NDI oligomers in bulk

NDI oligomers were expected to phase-separated into either stretched or folded conformers, depending on the unsaturated bonds in the spacer (Figure 3a). To get a better understanding of their packing in bulk, SAXS measurements in medium- (MAXS) and wide-angle (WAXS) operating modes were performed. In Figure 3b, the scattering profiles of the NDI oligomers are shown, and the data is summarized in Table 2. In addition, the scattering profiles of the pristine unsaturated diamines were recorded as reference data (Figure S5). All NDI oligomers, except **C_3-NDI_3** and **C_{12}-NDI_3**, were heated above their T_m and slowly cooled to room temperature prior to the scattering measurements to eliminate kinetically trapped states. **C_3-NDI_3** and **C_{12}-NDI_3** were annealed at 160 °C instead. The oligomers of sets 1 and 2 showed a principal scattering peak (q^*), with subsequent reflection peaks spaced at integer multiples ($2q^*$–$6q^*$), which is indicative of lamellar ordering. In the WAXS regime ($7 < q < 25\ nm^{-1}$), all NDI oligomers show very similar reflection patterns, indicating similar packing of the NDI cores. The sharp peak at 18.3 nm^{-1}–19.0 nm^{-1} corresponds to a spacing of 0.33–0.34 nm (determined using $d = 2\pi/q$), which is assigned as the π-stacking distance of the NDI core.[39]

When comparing the MAXS region ($0.1 < q < 7\ nm^{-1}$) of all oligomers, it is observed that the tetramer NDIs from set 3 show broad and undefined primary scattering peaks q^* around 0.52–0.80 nm^{-1}. Only **u_2C_{34}-NDI_4** shows equidistant signals corresponding to a lamellar morphology with respect to this broad and undefined peak at 0.8 nm^{-1}. We expect that the long flexible linkers with *cis* isomers lead to disordered structures regardless of their crystalline periphery, the presence of which is indicated by the sharp peaks in the WAXS region. This observation highlights that the processing of precise oligomers by simple thermal annealing from an isotropic state does not

Table 2. Summarized data of the volume fraction, morphology and domain spacing for all NDI oligomers.

Entry	Compound	f_{NDI} [–]	Phase	$d_{spacing}$ [nm]	$d_{streched}$ [nm]
1	C_3-NDI_3	0.43	LAM	5.6	5.7
2	C_{12}-NDI_3	0.34	LAM	7.7	7.9
3	u_2C_{34}-NDI_2	0.24	LAM	7.9	7.9
4	u_2C_{33}-NDI_3	0.24	LAM	3.8	12.6
5	u_2C_{33}-NDI_5	0.25	LAM	3.7	22.1
6	u_2C_{34}-NDI_4	0.31	LAM	5.8	12.7
7	u_4C_{56}-NDI_4	0.27	DIS	9.4	15.3
8	u_6C_{78}-NDI_4	0.24	DIS	9.2	17.0
9	u_8C_{100}-NDI_4	0.21	DIS	12.0	20.0

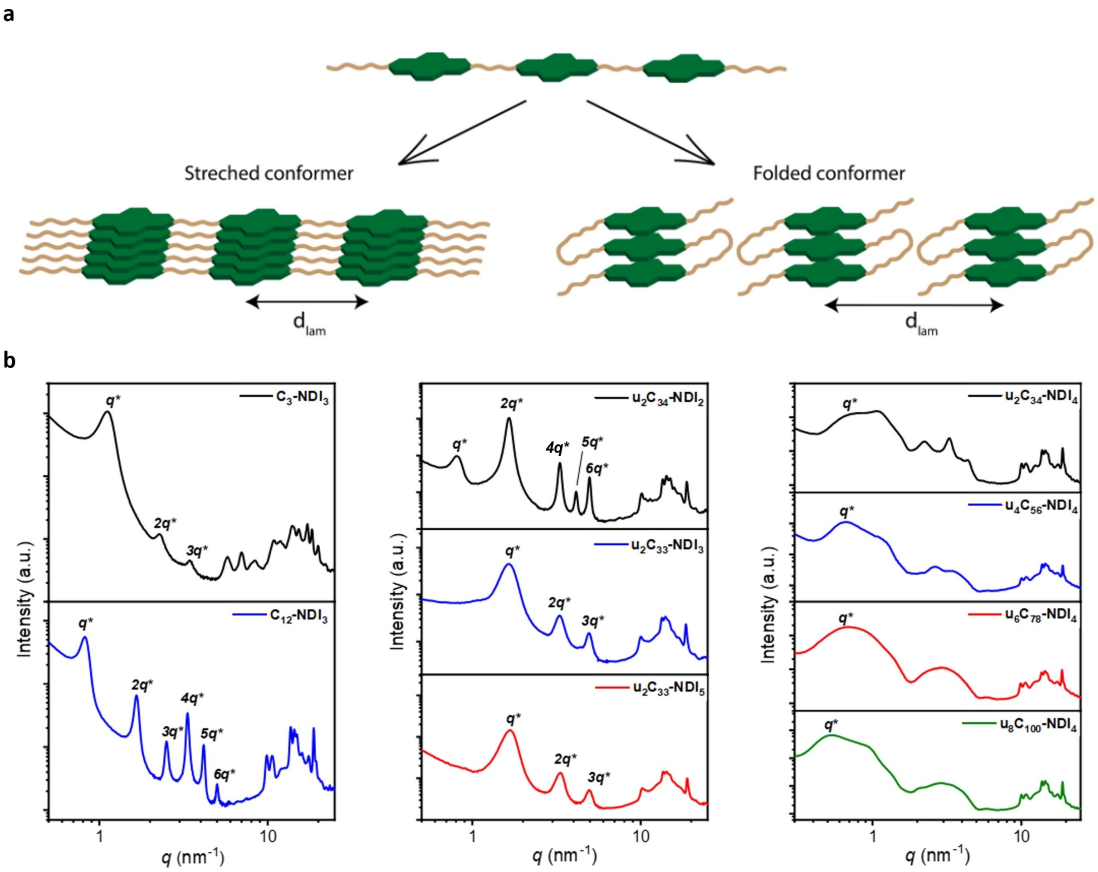

Figure 3. (a) Schematic representation of the possible conformations of NDI oligomers. (b) 1D transmission scattering profiles at room temperature for all NDI oligomers.

always result in well-defined bulk morphologies but requires more precision in the crystallization conditions.

Hereafter, we investigate the long-range order in the NDI oligomers by carefully evaluating the MAXS region ($0.5 < q < 7\ nm^{-1}$) of the scattering spectra. For all samples, the normalized linear one-dimensional correlation function $\gamma_{exp}(z)$ was computed by Fourier transformation of the background-subtracted Lorentz-corrected MAXS intensity. Defining z as the direction perpendicular to the lamellar packing, $\gamma_{exp}(z)$ is identical to the self-correlation $\gamma(z)$ of the electron density profile $\rho(z)$ of the lamellar structure averaged in planes perpendicular to z, $\rho(z) = \int \rho(x,y,z)dx\ dy$.[40] This correlation function comprises all direct-space information that can be obtained from the scattered intensity. It displays peaks at values corresponding to distances between structural elements repeated in the z direction, positive peaks arising from correlation between electron-richer or between electron-poorer regions of successive unit cells of the lamellar packing, whereas negative peaks arise from correlation between electron-richer and poorer regions (compared to the average electron density). Different possible theoretical electron density profiles were generated until the self-correlation function $\gamma(z)$ reproduced the main features of the experimental $\gamma_{exp}(z)$. The Lorentz-corrected intensity $I_1(q)$, experimental $\gamma_{exp}(z)$ and model $\gamma(z)$ correlation functions, and model electron density profiles of the unit cell in the z direction, $\rho_{RU}(z)$, are shown in Figure 4. For three oligomers of set 3, the correlation function rapidly dampens with distance, confirming the lack of long-range order also detected by the broadness of the scattering peaks. Hence, these samples are at least partially disordered under our crystallization conditions. It is expected that crystallization in an extended conformation should be possible under different crystallization conditions; however, the scattering of these samples was not analyzed further.

For the oligomers of set 1, the distance corresponding to the first Bragg reflection is in the range of the extended length of the molecules, and the experimental correlation functions can be well reproduced with model electron density profiles corresponding to a stretched conformation with tilted extended alkyl chains.[34] For **C_3-NDI$_3$**, the three NDI cores are not resolved separately in the electron density profile, owing to their spatial proximity in the crystals. In contrast, when the NDI cores are separated by 12 methylene units, they pack in layers sufficiently spaced apart to be resolved in the electron density profiles, which also explains the relative increase of intensity of the third and fourth order Bragg reflections in the MAXS intensity. Possible chain conformations corresponding to the electron density profiles of the crystals are displayed in Figure 4c.

The MAXS of oligomer **u_2C_{34}-NDI$_2$** of set 2 can be analyzed similarly. Its first order Bragg peak again indicates a stretched conformation with tilted alkyl chains, as supported by the electron density profile of its repeat unit. For this oligomer, the

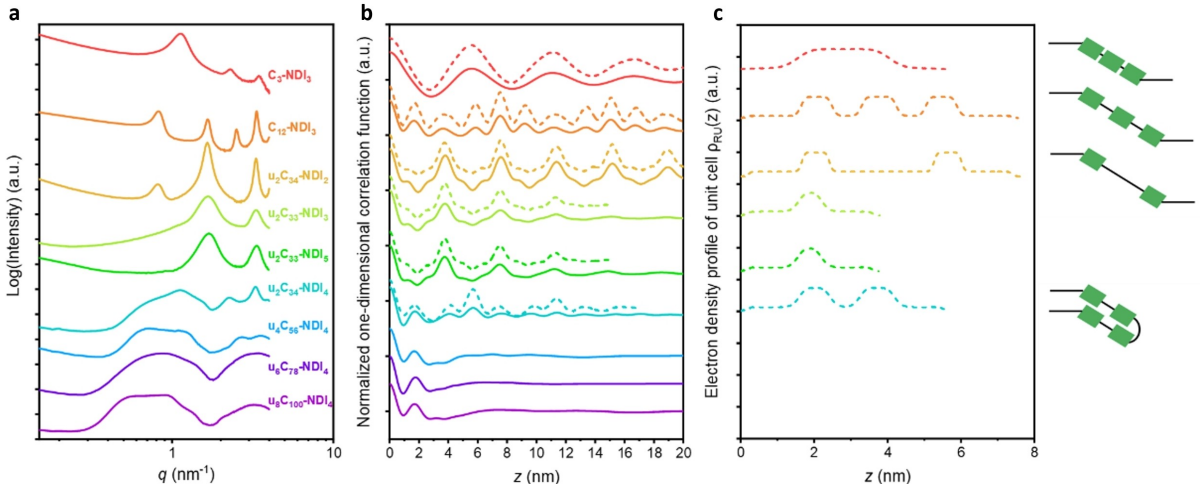

Figure 4. (a) Lorentz-corrected MAXS intensity ($I_1(q) = q^2\, I(q)$); (b) Normalized one-dimensional correlation function (continuous lines: experimental; dashed lines: computed from the model electron density profiles); (c) Model electron density profiles of the unit cell in the *z* direction, together with possible chain conformations.

higher intensity of the second order Bragg reflection arises from the correlation between the two NDI units belonging to the same molecule, which are spaced apart by *ca.* half the domain spacing. When extending the oligomer at both ends by extra dodecyl-NDI units to obtain oligomer **u_2C_{34}-NDI_4** of set 3, the first significant Bragg reflection corresponds to a domain spacing of 5.6 nm only (although a very weak shoulder at longer distance suggests the minority presence of another form of longer domain spacing). This is half the expected value, suggesting that the oligomer dominantly folds to form once-folded crystals, which is supported by the electron density profile (Figure 4c). This would also explain the presence of two melting endotherms in the DSC trace of this sample (Figure 2), the first endotherm corresponding to the melting of these once-folded crystals, whereas the second one would be associated to the melting of extended chain crystals formed by melting-recrystallization during the DSC scan.

Finally, samples **u_2C_{33}-NDI_3** and **u_2C_{33}-NDI_5** of set 2 have very similar scattering profiles and correlation functions, despite being of significantly different molecular lengths. Their first order Bragg peak coincides with the distance between two successive NDI units, and the correlation between these units rapidly fades with distance. Their DSC traces also exhibit multiple melting endotherms. Therefore, we surmise that these oligomers also adopt multiply-folded chain conformations in the crystals, resulting in a rapid loss of correlation between NDI units due to the looser stacking of folded chain crystals. Owing to the influence of disordering mechanisms in these two samples, it becomes difficult to identify a specific chain conformation in the crystals.

To obtain deeper insight into the different conformational ordering in bulk of the NDI oligomers, variable temperature (VT)-SAXS experiments were performed with **u_2C_{33}-NDI_3** (set 2, Figure 5). When **u_2C_{33}-NDI_3** is heated beyond T_{OOT} (> 96 °C), a new reflection peak (q') appears at 0.87 nm^{-1} (third order at 2.36 nm^{-1}),

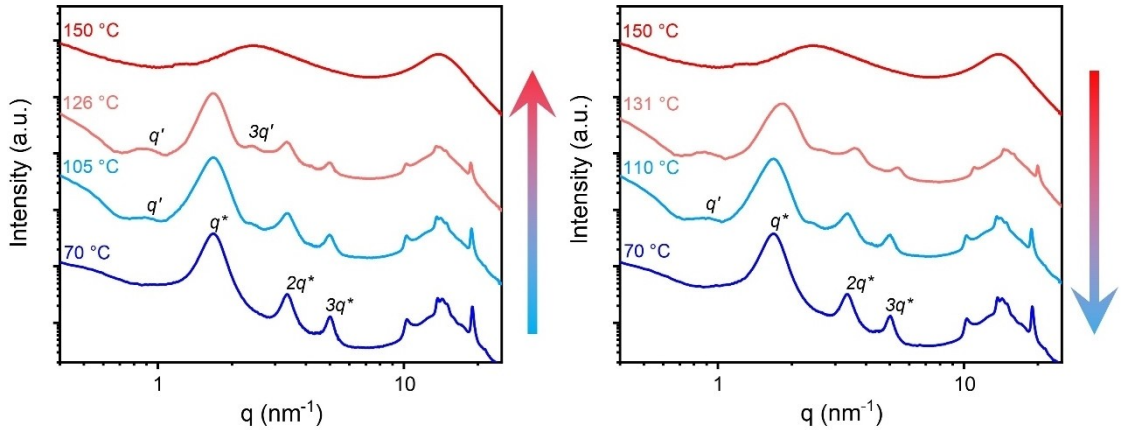

Figure 5. Variable-temperature SAXS profile of **u_2C_{33}-NDI_3** with a heating (*left*) and cooling (*right*) cycle. After measuring at each set temperature, the sample was brought to the next temperature using a 5 K min^{-1} ramp.

coinciding with a doubling of the unit cell in the *z* direction. The possible presence of a reflection at an even longer Bragg distance is suggested by the strong increase of the scattered intensity in the 0.4–0.6 nm^{-1} range. Heating over T_2 (122 °C) but below T_m (135 °C), the new set of reflection peaks become more intense and sharper, while the original reflections (q^*–$3q^*$) decrease in intensity. In addition, the peaks in the WAXS-region become slightly less-defined. This suggests the emergence of crystals involving less folded chain conformations. When **u_2C_{33}-NDI_3** is heated over T_m, the molecular ordering fully disappears. During the cooling measurements, it is observed that a reversible path is followed, which means that the folded conformation is thermodynamically favorable under these conditions, or that it is kinetically favored by the self-poisoning of the most stable form as reported for other precise oligomers.[41] These data show the rich conformational isomerism of NDI oligomers, which can assemble into several different folded or extended conformations, as well as mixtures of these phases.

Assembly of NDI oligomers at the liquid/HOPG interface

The highly ordered structures characterized for **C_{12}-NDI_3 and u_2C_{34}-NDI_2** prompted us to investigate their assembly at the liquid/HOPG interface. Figure 6 shows STM images of the self-assembled molecular networks formed upon physisorption of **C_{12}-NDI_3** and **u_2C_{34}-NDI_2** at the 1-phenyloctane (1-PO)/HOPG interface, where both systems form lamellar assemblies. Figures 6a and b shows the large- and small-scale STM images of SAMNs of **C_{12}-NDI_3**, respectively. The image consists of bright columns separated by darker ones. Interestingly, as anticipated from the molecular structure of **C_{12}-NDI_3**, the bright columns appear in groups of three, are equidistant, and are separated by a wider dark column. Thus, we ascribe the bright columns to the NDI cores of **C_{12}-NDI_3** and the wider dark columns to the areas where the terminal octadecyl chains are adsorbed. The narrow dark regions in between the triple bright columns can thus be attributed to the dodecyl spacer.

While the terminal octadecyl chains could not be resolved in the STM images obtained in 1-PO, STM data obtained at the 1,2,4-trichlorobenezene/HOPG interface reveal that the terminal chains from adjacent **C_{12}-NDI_3** columns acquire a non-colinear conformation (Figure S6). This type of packing was previously observed for the corresponding double NDI derivative with the same alkyl spacer.[31] The small scale STM image reveals that the bright columns are composed of circular features with a size of approximately 0.9 nm. These features are in good agreement with size of the NDI core obtained from the crystallography data and also agrees well with the size obtained from molecular models (Figure 6c). Occasionally the triple bright columns are adsorbed adjacent to each other without the typical wide dark column corresponding the octadecyl chains (Figure 6a, see top right). We ascribe this to the desorption of the terminal chains

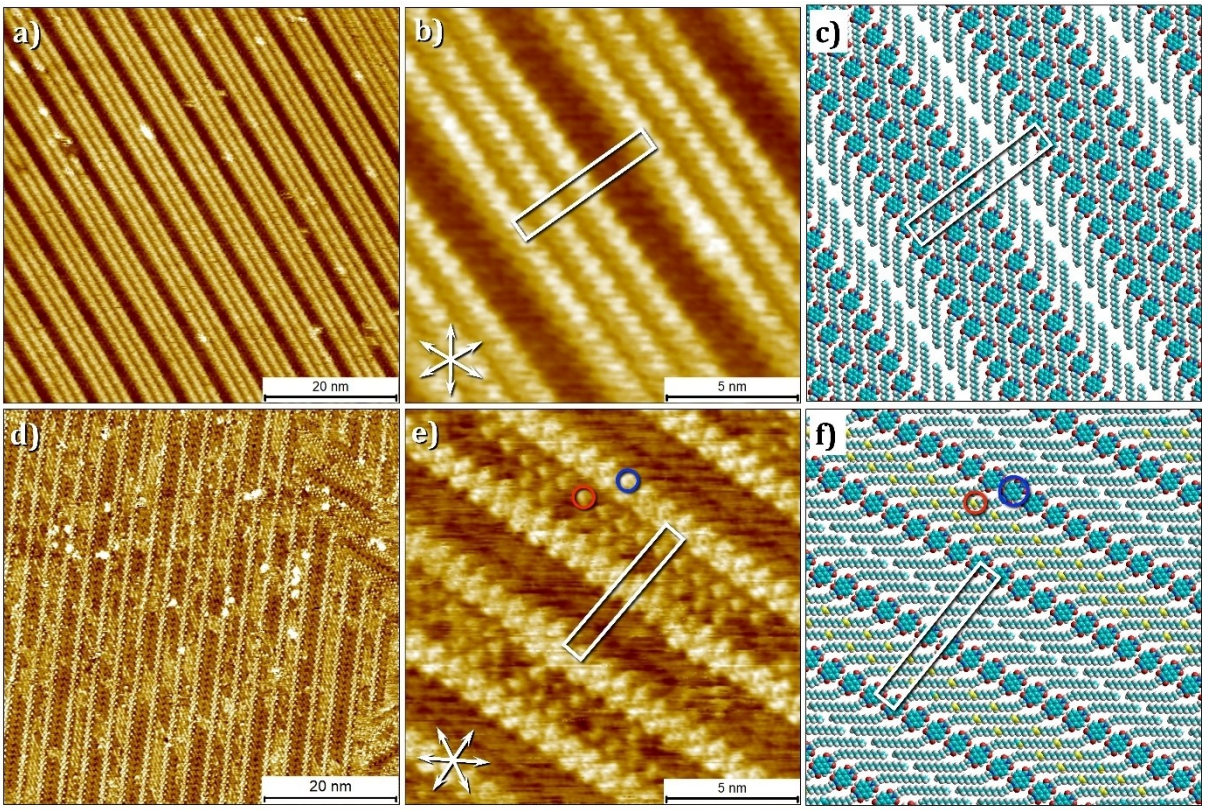

Figure 6. STM images of **C_{12}-NDI_3** (a, b) and **u_2C_{34}-NDI_2** (d, e) at the 1-phenyloctane/HOPG interface. (a, d) Large scale images, (b, e) high resolution images, (c, f) Corresponding tentative models. Imaging parameters : (a, b): $V_{bias} = 1.3$ V, $I_{set} = 0.05$ nA, (d, e): $V_{bias} = -1.45$ V, $I_{set} = 0.08$ nA.

from the surface, in which case they are backfolded in the supernatant solution.

Figures 6d and e shows STM images of the SAMN formed by **u_2C_{34}-NDI_2** at the 1-PO/graphite interface. In contrast to the self-assembled networks of previously investigated double NDI derivatives,[31] **u_2C_{34}-NDI_2** does not form the typical double lamellar structures. Instead, the bright columns, which can be attributed to the NDI cores, are equally spaced out similar to a single NDI derivative with the main difference being presence of a visible alternation in brightness of the darker columns in between. A high-resolution STM image of the network provided in Figure 6e reveals the presence of bright protrusions within the darker columns. These features are slightly smaller in size and less bright (red circle, Figure 6e) compared to those arising from the NDI cores (blue circle, Figure 6e). We ascribe these bright protrusions to the trans isomer of the double bonds present in the C_{33}-alkyl spacer, which are known to appear bright in STM images, and to adsorb preferentially to the cis isomer.[42,43] These data suggest the tail-to-tail extended conformation of **u_2C_{34}-NDI_2** on the surface (Figure 6f). However, another possible explanation for these protrusions is that one side of the molecule comprises adjacent C_{18}-chains, while the other end consists of a folded u_2C_{34}-chain, as proposed in the SAXS analysis. This alternative seems unlikely because alkyl chains are known to adsorb in an extended conformation on graphite surface as it is energetically favorable. Furthermore, it is well known that the chains have a specific registry with the substrate lattice[44,45] and hence they are almost always oriented along one of the main symmetry axes of graphite lattice. Any deviation from such registry is energetically unfavorable. However, we also note that bent conformations have been reported albeit rather rarely,[46] and complete folding of the chains as inferred from the SAXS analysis has also been reported although for specially designed systems such as foldamers.[47] The unit cell parameters of **u_2C_{34}-NDI_2** are $a = 0.9 \pm 0.1$ nm, $b = 6.2 \pm 0.3$ nm, and $\gamma = 89 \pm 1°$.

The large scale STM image provided in Figure 6d also indicates intermixing of the double bond containing spacers within the regions where terminal alkyl chains are adsorbed. This indicates that the molecules of **u_2C_{34}-NDI_2** do not stack perfectly and in fact show regular shifts as depicted in the molecular model provided in Figure S7. The clustering of the bright features corresponding to the double bonds indicates that the shift occurs in a cooperative fashion. The molecular model presented in Figure S7b indicates that such shifts are possible due to the close match between the length of the **u_2C_{34}**-spacer and combined length of the two terminal alkyl chains oriented in a non-colinear fashion. As both spacer and terminal alkyl chains stack parallel to each other, we expect that the two double bonds within the spacer possess *trans* geometry. It follows that the structure is selective towards only one conformation of the unsaturated spacer alkyl chain. We observed that such imperfect regions get removed upon annealing of the sample and the network becomes more regular.

To provide a proper comparison between the investigated saturated and non-saturated NDI derivates, we additionally investigated the self-assembly of **u_2C_{33}-NDI_3** at the 1-PO/HOPG interface. As shown in Figure S8, it forms a similar packing to **u_2C_{34}-NDI_2** with the spacing of the bright columns being equal in length despite the presence of a spacer which differs in length from a single terminal alkyl chain. As all alkyl chains appear to follow only one conformation as shown in the high-resolution image in Figure S8b, the alkyl spacers would also be required to possess only double bonds with a trans conformation.

Conclusions

The synthesis and assembly of a library of discrete alkyl-bridged NDI oligomers was presented. All three sets of discrete oligomers were obtained pure but in limited quantity due to the extensive synthetic effort. Nevertheless, detailed analysis showed that the molecular design of the NDI oligomers logically has a paramount role in the molecular properties in both solution and bulk. In general, the NDI oligomers tend to form lamellar morphologies via crystallization-driven assembly. The oligomers with shorter linkers preferably assemble in an extended conformation, while the oligomers with longer linkers show a mixture of folded-chain conformations and disordered morphologies due to the presence of the unsaturated spacers. The self-assembly of selected NDI oligomers was studied at the solution-solid interface using STM and revealed that the *trans* oligomers selectively adsorb in an extended conformation on the surface, leading to well-defined regions.

With this work, we gain insights into the influence of molecular design on the nanostructures of precise oligomer materials. Next to the challenge to synthesize these precise oligomers, the results have shown that the formation of long-range ordered structures is not trivial because complex assemblies can occur. The presence of long unsaturated alkyl chains, necessary for better solubility, simultaneously leads to entropic effects with the formation of folded conformations. To also achieve a high degree of precision in morphology, it is therefore essential to apply precise crystallization conditions to control the assembly pathway. With this study the frontiers in oligomer synthesis, molecular analysis, and ordered supramolecular assemblies of precise oligomer materials are pushed forward, while at the same time the limitations in this endeavor are made clear.

Experimental Section

Details on synthesis, characterization of synthesized molecules, additional UV-Vis and fluorescence spectra, details of the thermal and morphological analysis, and STM results are provided in the Supporting Information.

Supporting Information

The authors have cited additional references within the Supporting Information.[37,48–58]

Acknowledgements

The work received funding from the Belgian National Fund for Scientific Research (EOS Project Precision 30650939), European Research Council (H2020-EU.1.1., SYNMAT project, ID 788618), the Dutch Ministry of Education, Culture and Science (Gravitation Program 024.001.035 and NWO-M grant OCENW.M20.256), KU Leuven (C14/19/079), and the Research Foundation – Flanders (G0H2122N, EOS 30489208).

Conflict of Interests

The authors declare no conflict of interest.

Data Availability Statement

The data that support the findings of this study are available in the supplementary material of this article.

Keywords: Liquid-solid interface · nanostructure · naphthalenediimide · oligomer · self-assembly

[1] B. van Genabeek, B. A. G. Lamers, C. J. Hawker, E. W. Meijer, W. R. Gutekunst, B. V. K. J. Schmidt, *J. Polym. Sci.* **2021**, *59* (5), 373–403.
[2] G. M. Whitesides, B. Grzybowski, *Science.* **2002**, *295* (5564), 2418–2421.
[3] G. M. Whitesides, *Small* **2005**, *1* (2), 172–179.
[4] J. V. Barth, G. Costantini, K. Kern, *Nature* **2005**, *437*, 671–679.
[5] D. P. Goronzy, M. Ebrahimi, F. Rosei, Arramel, Y. Fang, S. De Feyter, S. L. Tait, C. Wang, P. H. Beton, A. T. S. Wee, P. S. Weiss, D. F. Perepichka, *ACS Nano* **2018**, *12* (8), 7445–7481.
[6] R. H. Zha, G. Vantomme, J. A. Berrocal, R. Gosens, B. F. M. de Waal, S. C. J. Meskers, E. W. Meijer, *Adv. Funct. Mater.* **2018**, *28* (1), 1–8.
[7] F. Lancia, A. Ryabchun, N. Katsonis, *Nat. Chem. Rev.* **2019**, *3* (9), 536–551.
[8] D. Dattler, G. Fuks, J. Heiser, E. Moulin, A. Perrot, X. Yao, N. Giuseppone, *Chem. Rev.* **2020**, *120* (1), 310–433.
[9] S. V. Bhosale, C. H. Jani, S. J. Langford, *Chem. Soc. Rev.* **2008**, *37* (2), 331–342.
[10] M. Al Kobaisi, S. V. Bhosale, K. Latham, A. M. Raynor, S. V. Bhosale, *Chem. Rev.* **2016**, *116* (19), 11685–11796.
[11] M. Ichikawa, K. Iwasaki, A. Ohyama, J. Miyazawa, Y. Yokota, N. Hirata, N. Oguma, *Jpn. J. Appl. Phys.* **2017**, *56* (11).
[12] D. Shukla, S. F. Nelson, D. C. Freeman, M. Rajeswaran, W. G. Ahearn, D. M. Meyer, J. T. Carey, *Chem. Mater.* **2008**, *20* (24), 7486–7491.
[13] A. Welford, S. Maniam, E. Gann, X. Jiao, L. Thomsen, S. J. Langford, C. R. McNeill, *Org. Electron.* **2019**, *75* (May), 105378.
[14] R. Niu, C. Pan, Z. Chen, L. Wang, L. Wang, *Chem. Eng. J.* **2020**, *381 (August 2019)*, 122650.
[15] Y. Wang, T. Hasegawa, H. Matsumoto, T. Mori, T. Michinobu, *Adv. Funct. Mater.* **2017**, *27* (33), 1–11.
[16] C. Fu, H. P. Lin, J. M. Macleod, A. Krayev, F. Rosei, D. F. Perepichka, *Chem. Mater.* **2016**, *28* (3), 951–961.
[17] D. A. Vicie, D. T. Odom, M. E. Núñez, D. A. Gianolio, L. W. McLaughlin, J. K. Barton, *J. Am. Chem. Soc.* **2000**, *122* (36), 8603–8611.
[18] A. Das, S. Ghosh, *Chem. Commun.* **2016**, *52* (42), 6860–6872.
[19] F. K. Zhan, S. M. Hsu, H. Cheng, H. C. Lin, *RSC Adv.* **2015**, *5* (60), 48961–48964.
[20] C. Kulkarni, S. J. George, *Chem. Eur. J.* **2014**, *20* (16), 4537–4541.
[21] M. R. Molla, D. Gehrig, L. Roy, V. Kamm, A. Paul, F. Laquai, S. Ghosh, *Chem. Eur. J.* **2014**, *20* (3), 760–771.
[22] H. Yan, Z. Chen, Y. Zheng, C. Newman, J. R. Quinn, F. Dötz, M. Kastler, A. Facchetti, *Nature* **2009**, *457* (7230), 679–686.
[23] X. Guo, M. D. Watson, *Org. Lett.* **2008**, *10* (23), 5333–5336.
[24] R. Scott Lokey, B. L. Iverson, *Nature* **1995**, *375* (6529), 303–305.
[25] V. J. Bradford, B. L. Iverson, *J. Am. Chem. Soc.* **2008**, *130* (4), 1517–1524.
[26] P. Ganesan, B. Van Lagen, A. T. M. Marcelis, E. J. R. Sudholter, H. Zuilhof, *Org. Lett.* **2007**, *9* (12), 2296–2300.
[27] B. Narayan, C. Kulkarni, S. J. George, *J. Mater. Chem. C* **2013**, *1* (4), 626–629.
[28] N. L. Ha, Z. Xu, K. K. Sook, K. M. K. Swamy, Y. Kim, S. J. Kim, J. Yoon, *J. Am. Chem. Soc.* **2007**, *129* (13), 3828–3829.
[29] J. A. Berrocal, R. H. Zha, B. F. M. De Waal, J. A. M. Lugger, M. Lutz, E. W. Meijer, *ACS Nano* **2017**, *11* (4), 3733–3741.
[30] W. Yang, D. Liu, Y. Liu, S. Yang, Y. Liu, Z. Shen, H. Yang, X. H. Fan, Q. F. Zhou, *Chem. A Eur. J.* **2023**, *29* (18).
[31] A. T. Rösch, R. Reynaerts, B. A. G. Lamers, K. S. Mali, S. De Feyter, A. R. A. Palmans, E. W. Meijer, *Chem. Mater.* **2021**, *33* (22), 8800–8811.
[32] Y. Miyake, T. Nagata, H. Tanaka, M. Yamazaki, M. Ohta, R. Kokawa, T. Ogawa, *ACS Nano* **2012**, *6* (5), 3876–3887.
[33] J. A. Berrocal, G. H. Heideman, B. F. M. De Waal, M. Enache, R. W. A. Havenith, M. Stöhr, E. W. Meijer, B. L. Feringa, *J. Am. Chem. Soc.* **2020**, *142* (8), 4070–4078.
[34] J. A. Berrocal, G. Henrieke Heideman, B. F. M. de Waal, E. W. Meijer, B. L. Feringa, *ACS Nano* **2020**, *14* (10), 13865–13875.
[35] K. Tambara, N. Ponnuswamy, G. Hennrich, G. D. Pantoş, *J. Org. Chem.* **2011**, *76* (9), 3338–3347.
[36] F. A. Carey, R. J. Sundberg, *Advanced Organic Chemistry, Part B: Reaction and Synthesis, Vol 1*, Springer New York, Boston, MA, **2007**.
[37] B. Van Genabeek, B. F. M. De Waal, A. R. A. Palmans, E. W. Meijer, *Polym. Chem.* **2018**, *9* (20), 2746–2758.
[38] G. Knothe, R. O. Dunn, *J. Am. Oil Chem. Soc.* **2009**, *86* (9), 843–856.
[39] B. A. G. Lamers, M. H. C. Van Son, F. V. De Graaf, B. W. L. Van Den Berssel-laar, B. F. M. De Waal, K. Komatsu, H. Sato, T. Aida, J. A. Berrocal, A. R. A. Palmans, G. Vantomme, S. C. J. Meskers, E. W. Meijer, *Mater. Horiz.* **2022**, *9* (1), 294–302.
[40] F. J. Balta-Callega, C. G. Vonk, *X-Ray Scattering of Synthetic Polymers, 11th ed.*, Elsevier, Amsterdam, **1989**.
[41] G. Ungar, X. B. Zeng, *Chem. Rev.* **2001**, *101* (12), 4157–4188.
[42] K. S. Mali, B. Van Averbeke, T. Bhinde, A. Y. Brewer, T. Arnold, R. Lazzaroni, S. M. Clarke, S. De Feyter, *ACS Nano* **2011**, *5* (11), 9122–9137.
[43] T. Arnold, S. M. Clarke, *Langmuir* **2008**, *24* (7), 3325–3335.
[44] A. J. Groszek, *Proc. Roy. Soc. Lond. Ser. A* **1970**, *314* (1519), 473–498.
[45] J. Dai, D. Wang, M. Zhang, T. Niu, A. Li, M. Ye, S. Qiao, G. Ding, X. Xie, Y. Wang, P. K. Chu, Q. Yuan, Z. Di, X. Wang, F. Ding, B. I. Yakobson, *Nano Lett.* **2016**, *16* (5), 3160–3165.
[46] M. G. Schwab, M. Takase, A. Mavrinsky, W. Pisula, X. Feng, J. A. Gámez, W. Thiel, K. S. Mali, S. De Feyter, K. Müllen, *Chem. Eur. J.* **2015**, *21* (23), 8426–8434.
[47] C. Gobbo, M. Li, K. S. Mali, J. H. Van Esch, S. De Feyter, *ACS Nano* **2012**, *6* (12), 10684–10698.
[48] Z. Chen, B. Fimmel, F. Würthner, *Org. Biomol. Chem.* **2012**, *10* (30), 5845–5855.
[49] M. S. Refat, I. Grabchev, J. M. Chovelon, G. Ivanova, *Spectrochim. Acta Part A* **2006**, *64* (2), 435–441.
[50] S. Alp, Ş. Erten, C. Karapire, B. Köz, A. O. Doroshenko, S. Içli, *J. Photochem. Photobiol. A* **2000**, *135* (2–3), 103–110.
[51] M. B. Avinash, T. Govindaraju, *Nanoscale* **2011**, *3* (6), 2536–2543.
[52] M. Pandeeswar, T. Govindaraju, *RSC Adv.* **2013**, *3* (29), 11459–11462.
[53] T. D. M. Bell, S. V. Bhosale, C. M. Forsyth, D. Hayne, K. P. Ghiggino, J. A. Hutchison, C. H. Jani, S. J. Langford, M. A. P. Lee, C. P. Woodward, *Chem. Commun.* **2010**, *46* (27), 4881–4883.
[54] M. Kumar, S. J. George, *Nanoscale* **2011**, *3* (5), 2130–2133.
[55] D. B. Shaikh, K. S. More, M. Al Kobaisi, D. D. La, S. V. Bhosale, S. V. Bhosale, *ChemistrySelect* **2020**, *5* (44), 14203–14209.
[56] M. R. Molla, S. Ghosh, *Chem. Eur. J.* **2012**, *18* (5), 1290–1294.
[57] P. Sharma, S. Kaur, S. Kaur, P. Singh, *Photochem. Photobiol. Sci.* **2020**, *19* (4), 504–514.
[58] S. Maity, M. Shyamal, P, Mazumdar, G. P. Sahoo, R. Maity, G. Salgado-Morán, A. Misra, *J. Mol. Liq.* **2016**, *224*, 255–264.

Manuscript received: September 25, 2023
Accepted manuscript online: November 27, 2023
Version of record online: December 19, 2023